Pergamon

Geochimica et Cosmochimica Acta, Vol. 68, No. 11, pp. 2495–2507, 2004

0016-7037/04 $30.00 + .00

doi:10.1016/j.gca.2003.11.003

Experimental growth of quartz in petroleum environment. Part I: Procedures and Fluid Trapping

STÉPHANE TEINTURIER*,† and JACQUES PIRONON
UMR G2R-CREGU, UHP BP23 F-54506 Vandoeuvre-lès-Nancy Cedex, France

(*Received February* 20, 2003; *accepted in revised form November* 5, 2003)

Abstract—The quartz-water-oil-gas system has been experimentally studied with the objective of investigating the trapping of petroleum and aqueous inclusions in quartz at different water/oil (W/O) ratios (0/100, 5/95, 10/90, 20/80, 50/50, 100/0). Experiments were carried out in both a gas-pressure autoclave (GPA) under CH_4 pressure control, up to 250°C and 212 bar, and in a fluid-pressure autoclave (FPA) up to 350°C and 400 bar. High p-T conditions have notably allowed the growth of quartz at high oil saturation levels (W/O ratios from 10/90 to 50/50). Petroleum inclusions have been synthesised inside quartz microfractures (W/O ratios from 0/100 to 50/50; 209–350°C; 175–400 bar), and also inside quartz overgrowths (W/O ratios from 10/90 to 50/50; 289–350°C; 350–400 bar). Aqueous inclusions have been synthesised in presence of oil inside quartz microfractures from 185°C-163 bar up to 400°C-400 bar, and inside quartz overgrowth from 277°C-330 bar. Synthesised petroleum inclusions are representative of the parent oil up to 250°C. At 350°C, evidence of a cracking process has been observed with the consequent formation of methane. The segregation of the oil/gas/water column inside the GPA autoclave may also have prevented methane diffusion into the water phase when oil is present. This experimental approach shows that the trapping of fluid inclusions and the formation of quartz cement, under conditions of high oil saturation, have not been suppressed or prevented.

1. INTRODUCTION

In a quartz-rich sandstone that is quartz cemented, petroleum and aqueous inclusions can be very useful in deciphering the history of a natural petroleum reservoir. The quartz precipitation and fluid inclusion trapping are not always synchronous. Re-equilibration, necking of the fluid inclusions or the mode of trapping can often obscure the relationship and chronology between the healing of fracture, growth of quartz and petroleum migration (Haszeldine and Osborne, 1993; Teinturier et al., 2002). On the other hand, the ability of petroleum emplacement to inhibit quartz cementation is, as yet, an unknown. This has been debated by many authors and depends mostly on the controls on silica transport from its source to precipitation (Worden and Morad, 2000). An oversaturated silica-solution is always required to create quartz overgrowths with fluid inclusions, whereas the healing of a microfracture with fluid inclusions (which may not need the addition of new quartz) needs at least a local dissolution-re-precipitation process. Although no experimental studies have confirmed this tendency, the concept that quartz cementation is inhibited or retarded by oil emplacement has been empirically demonstrated in several oil fields, and is based on significant differences in porosity of some oil-bearing sandstones reservoirs in otherwise texturally and compositionally identical sandstones (Dixon et al., 1989; Gluyas et al., 1993; Marchand et al., 2001; Marchand et al., 2002). If new quartz cannot grow with oil, the presence of petroleum inclusions could be explained by possible quartz porosity filling after the formation of quartz overgrowths, especially at the core-overgrowth boundary (Barclay and Worden, 2000; Larese and Hall, 1996; Meunier, 1992). In contrast, the presence of petroleum inclusions inside quartz cements, similar homogenisation temperature ranges and/or relative volumes of cement and porosities between water and oil-saturated zones are the prime empirical arguments of authors who consider that oil emplacement does not halt quartz cementation (Walderhaug, 1990; Ramm, 1992; Saigal et al., 1992; Midtbø et al., 2000).

Taking into account the numerous petroleum reservoirs studies, many problems, or misunderstandings, result from the lack of knowledge of the fluid inclusion formation processes when oil is present. In particular, we need more information on the kinetic and chemical parameters control fluid inclusion formation. The specific questions that require answers include: what oil saturation is necessary to give rise to petroleum inclusions with or without aqueous inclusions during quartz cementation? Is the composition of petroleum inclusions representative of the original fluid composition? Are fluid inclusions inside quartz overgrowths representative of the growth of quartz? These questions are addressed in this paper by synthesising petroleum inclusions under controlled experimental conditions.

Since the first experiments by Roedder and Kopp (1975), numerous syntheses of fluid inclusions have been produced in quartz microfractures and/or quartz overgrowths (e.g., Shelton and Orville, 1980; Sterner and Bodnar, 1984; Bodnar and Sterner, 1985; Zhang and Frantz, 1987; Dubois et al., 1994; Sawaki et al., 1997; Teinturier and Pironon, 2003). These experiments have been carried out at a range of temperatures (175 to 1000°C) and pressures (P_{sat} to 7 kbars) in different systems (pure H_2O, H_2O-NaCl, H_2O-NaOH, H_2O-LiCl, H_2O-CsCl, H_2O-KCl, H_2O-$CaCl_2$, H_2O-CO_2). The experimental time needed to form these aqueous inclusions was between 0 and 87 d. Other authors have synthesised fluid inclusions in the

* Author to whom correspondence should be addressed (Stephane.Teinturier@g2r.uhp-nancy.fr).
† *Present address:* CSIRO Petroleum, 26 Dick Perry Avenue, ARRC, Kensington, Perth, WA 6151 Australia.

H_2O-NaCl-CH_4 system at temperatures from 150 to 600°C and pressures from 0.1 to 1 kbar inside 30 d (Lamb et al., 1996; Dubessy et al., 2000b; Guillaume et al., 2003).

In contrast, relatively few experiments synthesising petroleum inclusions inside quartz have been performed. Larese and Hall (1996) produced synthetic petroleum inclusions with a variety of pore fluids ranging from 100% aqueous to 100% oil, within quartz microfractures, at the quartz overgrowth boundary and within overgrowth at conditions of 150, 325 and 360°C with a hydrostatic pressure of 690 bar over 12 d. Some inclusions, particularly those at the quartz overgrowth boundary were incompletely sealed during these experiments, resulting in porous, permeable interfaces which were accessible to later pore fluids in spite of significant overgrowth formation. Note that the growth of quartz required relative high temperatures (>300°C) to grow in the laboratory in few days. Vityk et al. (2001) also produced synthetic petroleum inclusions inside fractured core samples (not in neoquartz overgrowths) at 180°C and 480 bar over 10 d. Their experimental observations suggest that oil saturation appears to play a secondary role in inclusion abundance and distribution. Hydrocarbon inclusions have also been synthesized in halite salt crystals (Pironon, 1990; Stasiuk and Snowdon, 1997) at low temperature (<200°C).

In this study, we have attempted to produce synthetic petroleum and aqueous fluid inclusions during quartz precipitation, i.e., the healing of microfracture and formation of quartz overgrowth. These fluid inclusions have been characterised by different techniques: microthermometry, confocal scanning laser microscope (CSLM), Raman and infrared microspectroscopies. These observations were used as input to thermodynamic modelling with PIT software (Petroleum Inclusion Thermodynamics) (Thiéry et al., 2002), which allowed PVTX reconstruction of the trapping conditions of petroleum fluid.

2. INCLUSION SYNTHESIS

The experimental cementation of quartz and synthesis of fluid inclusions in the presence of variable proportions of petroleum and aqueous solution was investigated at temperatures and pressures up to 350°C and 400 bar. The experiments were carried out in autoclaves on both synthetic quartz (sticks of 1 cm in length and a square section of 0.3 mm) and natural Brazilian quartz crystals (<1 cm), which were cut perpendicular to their growth c-axis. Before the experiments were run, samples were heated to 700°C to eliminate any preexisting inclusions. The quartz was then fractured by soaking the heated quartz in cold distilled water and then dried for 6 h at 90°C.

The oil used in the experiment is a paraffinic oil, which contains 44 wt.% of saturated hydrocarbon. The aromatic fraction is 32 wt.% and the polar fraction (asphaltenes and resins) is 24 wt.% (Teinturier et al., 2003). Oil density is 878.5 kg/m^3 at 15°C, and under laboratory conditions (1 bar, 20 C) does not contain the any gas (methane, nitrogen, and carbon dioxide) or volatile hydrocarbons (C_2 to C_5). Therefore, the proportion of heavy molecular weight hydrocarbons is higher in the laboratory sample than in the natural crude oil under reservoir conditions.

Two types of autoclaves (Autoclave Engineering Closure) were used, depending on the p-T conditions and autoclave limitations. Experiments with methane were carried out in a gas-pressure autoclave (GPA) up to 250°C and 212 bar. For higher temperatures and pressures, experiments were conducted in a sealed gold capsule, inside a fluid-pressure autoclave (FPA).

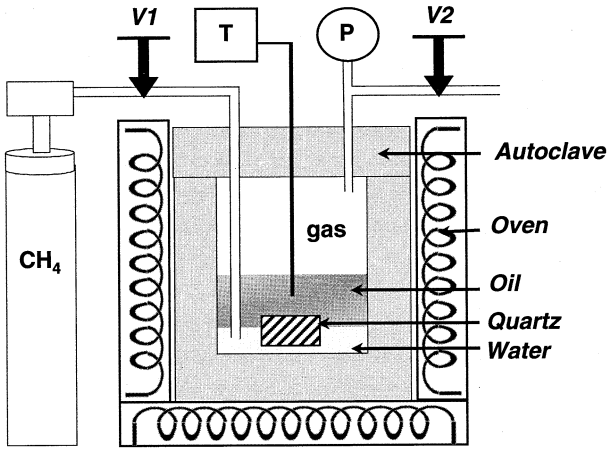

Fig. 1. Gas pressure autoclave (GPA).V1: inlet valve, V2: outlet valve, T: thermocouple, P: manometer.

In the GPA system, pressure within the experimental volume was regulated by the introduction of methane gas (Fig. 1). The major advantage of this autoclave design is to maintain the equilibrium between liquid and vapour phases at run conditions (Dubessy et al., 2000b; Guillaume et al., 2003). When a fluid inclusion entraps a single phase of an immiscible fluid in this experimental arrangement, the homogenisation temperature (T_h) of this inclusion is equal to the trapping temperature of the fluid inside the same inclusion (in an aqueous system). Quartz samples were introduced into the base of the autoclave and silica gel added. Depending on the experimental conditions, the oil and aqueous solution were added in various filling orders (Table 1). Some of the thicker synthetic quartz blocks contacted both the oil zone and the water zone. This last configuration encouraged the formation of aqueous and petroleum fluid inclusions in the same thick samples. Indeed, water and oil could access through the fracture network of the synthetic quartz. Methane was first introduced through valve V1 to purge the air contained in the gas and liquid phase. Afterwards, valve V2 was closed and the methane pressure was adjusted via V1 before the increase of temperature. The pressure inside the autoclave was thus higher than the saturated pressure in a pure or chloride-bearing water system. Temperature and pressure were constantly controlled and modified during of the experiments. At the end of the experiments, the autoclave was cooled to the ambient temperature over ~4 h and opened.

In the FPA system, fluid pressure was generated by a hydraulic pump and transmitted inside the autoclave by a water-oil mixture (Hydraulub 16 g/L) in a pressure line (Fig. 2). Quartz samples were placed inside gold capsules (L = 6 cm; i.d. = 0.5 cm), which are chemically inert and have good thermal conductivity and malleability. This favours the transfer of temperature and pressure. Gold tubes were welded at one end, then filled with the quartz samples, silica gel and oil/aqueous solution. The other end was welded while the tube was cooled in liquid nitrogen to prevent any alteration or loss of the

Table 1. Experimental conditions realised in the gas-pressure autoclave (GPA) and inside gold capsules in the fluid pressure autoclave (FPA). [1]Guillaume et al., (2003); [2](S: quartz sample, W: aqueous solution, HC: oil sample); [3]HF: healing fracture; [4](QO: quartz overgrowth, pyr.: quartz pyramids); [5]Raman detection.

Exp.	System[2]	Autoclave/bag filling order[2]	p-T conditions Maximum	p-T conditions Minimum	Duration (days)	Water-oil ratio[3]	Quartz cementation HF[4]	Quartz cementation QO[5]	Fluid inclusions Aqueous	Fluid inclusions Petroleum	Fluid inclusions Triphasic	CH_4 Aq. Inclusion[8]
Gas-pressure autoclave												
G1[1]	$CH_4+H_2O+NaCl$	S-W	250°C-200 bar	150°C-100 bar	20	100/0	yes	pyr.	yes	—	—	saturated
G2	$HC+CH_4+H_2O+NH_4Cl$	S-W-HC	250°C-212 bar	150°C-141 bar	30	10/90	yes	pyr.	yes	yes	no	undersaturated
G3	$HC+CH_4+H_2O+NH_4Cl$	S-HC-W	250°C-209 bar	150°C-136 bar	30	20/80	yes	pyr.	yes	yes	no	not detected
G4	$HC+CH_4+H_2O+NH_4Cl$	S-HC	250°C-200 bar	150°C-200 bar	25	0/100	no	no	no	no	no	—
G5	$HC+CH_4+H_2O+NaCl$	S-W-HC	270°C-200 bar		30	5/95	yes	pyr.	yes	yes	no	not detected
Fluid-pressure autoclave												
F1	$HC+H_2O+NaCl$	S-HC	350°C-400 bar		25	0/100	yes	pyr.	no	yes	no	—
F2	$HC+H_2O+NaCl$	S-W-HC	350°C-400 bar		25	5/95	yes	pyr.	yes	yes	no	not detected
F3	$HC+H_2O+NaCl$	S-W-HC	350°C-400 bar		25	10/90	yes	yes	yes	yes	yes	not detected
F4	$HC+H_2O+NaCl$	S-W-HC	350°C-400 bar		25	20/80	yes	yes	yes	yes	yes	not detected
F5	$HC+H_2O+NaCl$	S-W-HC	350°C-400 bar		25	50/50	yes	yes	yes	yes	yes	not detected
F6	$H_2O+NaCl$	S-W	350°C-400 bar		20	100/0	yes	yes	yes	—	—	—

solution. When oil was present, this procedure was performed under inert argon atmosphere to avoid oxidation of oil during the capsule preparation and the experiments. Before loading the capsules into the autoclave, they were weighed, heated to 150°C for 2 h and weighed again. The capsules showing a weight difference of 0.2% were discarded. Temperature was controlled by two thermocouples, one inside the oven and the other in the autoclave adjacent to the sample. Temperature and pressure were reached and stabilised in ~8 h. P-T conditions could be controlled at any time of the experiments. At the end of the run, the autoclave was cooled in 4 h and the capsules cleaned with chloroform and weighed. Contrary to the GPA system, no methane was supplied to the system.

Experimental conditions are shown in Table 1 for both type of autoclave. Experiments were conducted in aqueous and/or petroleum system, both with and without methane, with different ionic species such as NH_4^+, Cl^- or Na^+ and with silica gel. Different W/O ratios (0/100, 5/95, 10/90, 20/80, 50/50 and 100/0 at 25°C; ratios are weight %) have been used and different orders of filling of the autoclave have been tested. In this method quartz samples have been initially wetted with water or oil. The amount of silica gel added to the FPA capsules varies between 10 and 40 mg and can reach up to 20% of the total amount of minerals (quartz + silica gel). The average water content of this silica gel has been quantified around 10 wt.% by Raman spectroscopy (Chabiron et al., 2004). For the majority of the experiments, the rate of quartz precipitation has been enhanced by varying the temperature and the pressure. Maximum pressure and temperature were maintained for 5 to 10 d to saturate the solution in silica. After that, temperature and pressure were gradually reduced in a stepwise manner. This procedure aimed to oversaturate the solution at each step and enhance the occurrence of quartz precipitation and inclusion sealing. Experimental times were between 10 and 30 d. According to Tester et al. (1994), quartz solubility in pure liquid water increases with increasing pressure and temperature. For our p-T experimental condition range, the solubility of silica in NaCl solutions was higher than in pure water (Xie and Walther, 1993). The expected yield of quartz precipitation lies between 500 ppm at 250°C and 150 ppm at 150°C for the GPA experiments, and around 1000 ppm at 350°C-400 bar for the FPA experiments. The formation of quartz overgrowth should have been enhanced in the FPA system.

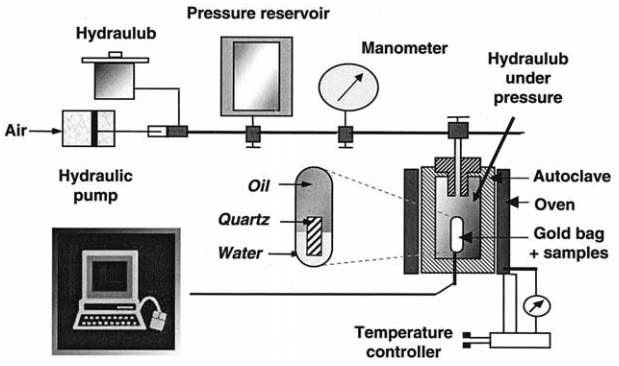

Fig. 2. Fluid-pressure autoclave (FPA).

Oxidation of oil was partially avoided by either purging air in the sample chamber by pressure transfer (GPA) or by loading and welding the gold capsules under an inert atmosphere (FPA). NH_4Cl was used in some experiments to maintain a redox potential thanks to the NH_4/N_2 equilibrium, which is similar to the hematite/magnetite buffer. A small amount of metallic iron was added to each solution to maintain a weak Eh at temperatures of around 250°C.

After the experiments were completed, the quartz samples were extracted from the aqueous and/or petroleum solution and cleaned with ethanol and dichloromethane to remove residual oil. The samples were manually polished to avoid destruction of any quartz overgrowth and/or fluid inclusions, especially near the surface.

3. ANALYTICAL METHODS

All samples were inspected under a standard polarising microscope equipped with fluorescence accessories (emission UV filter LP 400 nm long pass) to locate and separate the aqueous inclusions from the petroleum inclusions. Petroleum inclusions were identified by their fluorescence under ultraviolet illumination.

3.1. Microthermometry

Microthermometric data were acquired using a Chaix-Meca (Poty et al., 1976) for the melting temperatures (T_m), a USGS (Goldstein and Reynolds, 1994) for the homogenisation temperatures (T_h), and a Linkam MDS600 coupled to a video screen for the T_m and T_h. The measurement chambers of both the Chaix-Meca and USGS instruments are large enough to contain thick samples, which was useful for the synthetic quartz blocks. T_h measurement accuracy should be considered to be around ±2°C, which takes into account the potential thermal gradient between the thermocouple and the fluid inclusion area in thick quartz samples and high temperatures (350°C).

The fluid inclusion stages were calibrated by pure CO_2 inclusions (T_m = −56.6°C) and low salinity synthetic aqueous inclusion (T_m = −0.4°C) at low temperature, and by melting of various standards at higher temperatures.

3.2. Raman Microspectrometry

Methane detection and Raman quantitative analyses of aqueous inclusions were performed on a Labram Dilor spectrometer using incident radiation of 514.5 nm. The radiation was produced by an argon laser and coupled to a microscope equipped with a Linkam heating stage. Methane concentration in the liquid phase at T_h was determined using the calibration curves of Dubessy et al. (2000a) and Guillaume et al. (2003). Accumulation time, laser power and confocal aperture were adapted for each inclusion measurement to obtain the best signal/background ratio. Petroleum inclusions were too fluorescent to be analysed by Raman spectroscopy.

3.3. Fourier Transform Infrared Microspectrometry (FT-IR)

FT-IR spectra have been recorded using a Bruker Equinox 55 Fourier transform spectrometer. The infrared absorption of quartz prevents the investigation of the mid infrared range below 2000 cm^{-1}. The infrared beam was reduced to the bulk inclusion size with a variable diaphragm located in the image plane. The minimum apertures used were 20 μm using a ×15 objective, and 8 μm using a ×36 objective. The accumulation time was around 4 min and the spectral resolution is 4 cm^{-1}. Before each inclusion measurement, a reference spectrum was recorded in free air. Quartz contribution was partially removed by subtraction of its FT-IR spectrum, recorded in an area neighbouring the inclusions and free of contaminants (fluid inclusions and organic matter). Contributions of atmospheric H_2O and CO_2 were also removed by subtraction of their independently recorded characteristic spectra. FT-IR spectra of the oil sample were obtained by placing a small amount of oil between two polished CaF_2 slides. Analyses were made in transmission non-polarised mode.

Quantitative analysis of oils and petroleum inclusions was obtained according to the method of Pironon et al. (2001) and only accounts for the alkanes, CH_4 and CO_2. CO_2 is detected at 2340 cm^{-1}, CH_4 at 2960, 3006 and 3050 cm^{-1}, and the alkanes (CH_2- and CH_3-) at 2860, 2877, 2930 and 2960 cm^{-1}. The CH_2/CH_3 ratio is used to compare the free oil sample and the petroleum inclusions. Note that hydrocarbons are not strictly constituted by CH groups and the FT-IR approach has its own limitations. FT-IR analyses do not take into account the aromatics (C═C) and the polar compounds (C-O, C═O, N-. . .) due to the IR absorption of quartz. However, the CH_2 and CH_3 contributions are related to the presence of linear or branched alkanes, to aliphatic cycles, and to the aliphatic branches on aromatics and polar molecules. By consequence the measurement of the CH stretching band area covers much more than the *n*-alkanes.

3.4. Confocal Scanning Laser Microscopy (CSLM)

CSLM analyses (Pironon et al., 1998; Aplin et al., 1999) were performed at the Institut de Biologie Moléculaire des Plantes (IBMP) in Strasbourg, using a Zeiss (LSM 510) apparatus. The CSLM technique can estimate the volume of the cavity of an oil inclusion to an accuracy better than 95% with a spatial resolution lower than 0.5 μm (Pironon et al., 1998). The spatial resolution of CSLM is near to that of a standard scanning electron microscope (SEM). Besides conventional transmission observations, two other visual modes were used: (1) fluorescence mode using an incident laser radiation at λ_0=488nm and collecting emission of fluorescence at a longer wavelength of $\lambda > \lambda_0$. This mode is effective for liquid oil detection. (2) reflection mode using incident laser radiation and a filter in front of the collecting photomultiplier, both at 637 nm. This mode is very sensitive to refractive index changes and is used for the detection of liquid water inside inclusions because oil and quartz have similar indices and are both higher than the liquid water index (Teinturier et al., 2002). Confocal planes were acquired with a 0.5 μm step, and 3D reconstructions of the inclusions attained using image processing software. The volumes of the gas bubbles (Fv) were calculated, which is equivalent to the percentage of vapour inside the inclusion at a given temperature. In some rare and favourable cases, the volume of water within the inclusion was also estimated.

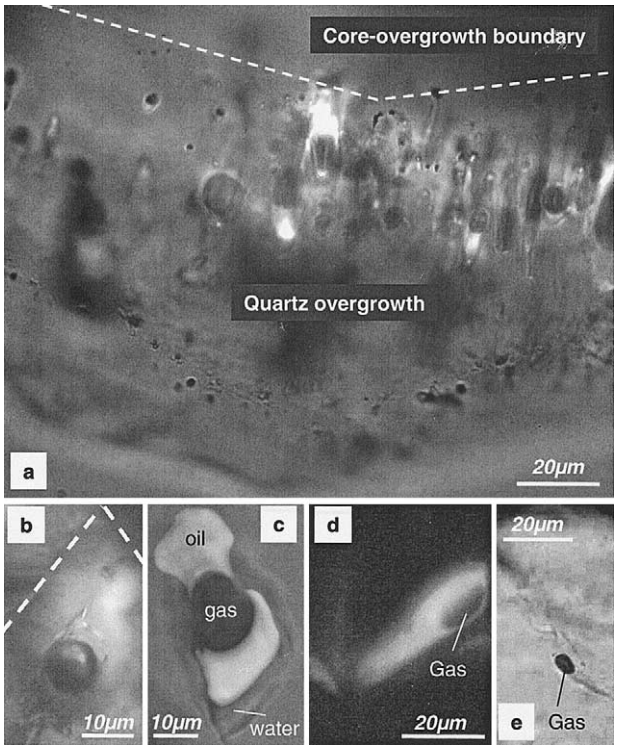

Fig. 3. Synthetic fluid inclusions in quartz. a, b: petroleum inclusions inside quartz overgrowth (F3 experiment, W/O ratio = 10/90). c: petroleum inclusions inside quartz microfractures (F5 experiment, W/O ratio = 50/50). d, e: petroleum (d) and aqueous (e) inclusions within healed microfractures (G2 experiment, W/O ratio = 10/90). All quartz are synthetic quartz except (b), which is natural Brazilian quartz.

4. RESULTS

4.1. Description of Fluid Inclusions

Synthetic petroleum, 3-phase petroleum (oil-gas-water at room temperature) and aqueous inclusions were produced in both the synthetic and natural Brazilian quartz samples (Fig. 3 and Table 1). In the FPA system, only a few petroleum inclusions were found in the Brazilian quartz compared to the synthetic quartz. In the GPA system, small petroleum inclusions were found only in synthetic quartz. As a consequence, this study was mainly focused on synthetic quartz.

Overall, the synthetic petroleum inclusions have sizes between 5 and 30 μm and often appear to be larger than aqueous inclusions (Fig. 3). The largest petroleum inclusion had a maximum size of around 75 μm. The vapour-liquid (-water)

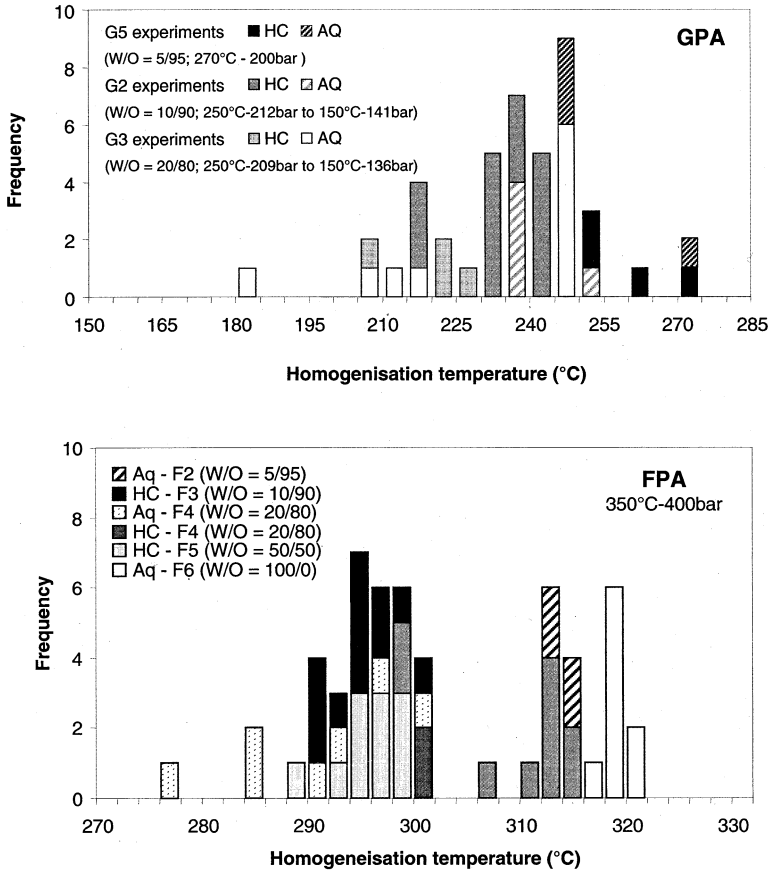

Fig. 4. Homogenisation temperatures (T_h) of synthetic aqueous and petroleum inclusions formed in the GPA and FPA systems.

ratio of the fluid inclusions were almost constant for each individual experiment, but more accurate data will be detailed further in the text (i.e., §4.5.).

Petroleum inclusions were located within healed microfractures (GPA and FPA experiments) and inside quartz overgrowth (FPA experiments only). Despite the absence of water in the F1 experiment (350°C-400 bar; W/O = 0/100), rare and tiny petroleum inclusions were observed within microfractures. This is not the case in the G4 experiment (250°C-200 bar; W/O = 0/100), where no fluid inclusions were found. When quartz samples were initially wetted by oil (G3 experiment), petroleum inclusions were rarely produced. Petroleum inclusions emplacement inside quartz overgrowth were mostly parallel (Fig. 3a,b) to the c-axis of the quartz. Depending on the experiment, the W/O ratio and the degree of cementation, petroleum inclusions located within healed microfractures were often tabular (Fig. 3d). The tabular nature of the inclusions was noticeable by the darkness and the non-sphericity of their gas bubbles at 25°C. Necking-down was observed locally between 2-phase and 3-phase petroleum (containing visible water) inclusions and between aqueous and 3-phase petroleum inclusions. The smallest necked inclusions were free of a gas bubble.

Aqueous inclusions from the GPA experiments were flat, biphasic and found within healed microfractures (Fig. 3e). These aqueous inclusions were rare in samples that were firstly wetted by water, and almost absent in samples that were firstly wetted by oil. In the FPA experiments, biphase synthetic aqueous-inclusions were found in the microfractures and within quartz overgrowths. Small, monophase synthetic aqueous-inclusions were also locally found in conjunction with petroleum inclusions close to the core-overgrowth boundary, and as isolated inclusions in the external part of the overgrowth (Fig. 3a).

4.2. Microthermometry

T_h diagrams for the GPA and the FPA experiments are shown in Figure 4. Results show that for most of the experiments, T_h values of synthetic aqueous and petroleum fluid inclusions are not homogeneous. The spread of T_h data mainly results from the decrease of the p-T conditions imposed inside the GPA, and the cooling of the FPA at the end of the experiments.

In the GPA experiments, the lowest and the highest measured T_h values were respectively 209°C (G5) and 274.6°C (G3) for synthetic petroleum inclusions, and 184.6°C (G3) and 270°C (G5) for synthetic aqueous inclusions.

In the FPA experiments, the maximum p-T trapping conditions of fluid inclusions were at 350°C and 400 bar in the monophase liquid domain. According to the equation of state (EOS) of Brown (1989) and Zhang and Frantz (1987), the maximum theoretical T_h of our synthetic aqueous fluid inclusions should have been between 320 and 332°C with a NaCl

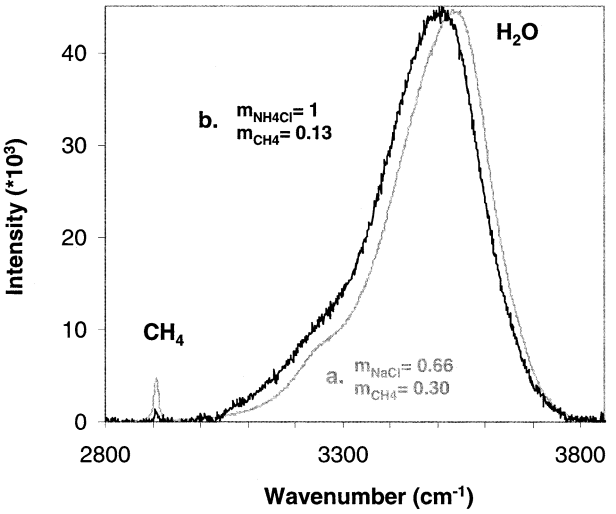

Fig. 5. Raman spectrum of two synthetic aqueous inclusions obtained in the liquid phase at the T_h (GPA). Both inclusions have been trapped in the presence of methane but aqueous inclusion "a" has been trapped without oil (G1 experiment, T_h-P_h = 234°C, 200 bar) whereas aqueous inclusion "b" has been trapped in the presence of oil (G2 experiment, W/O = 10/90, T_h-P_h = 237.3°C, 201 bar).

salinity of 1 molal. The maximum T_h values of the aqueous fluid inclusions trapped inside microfractures and quartz overgrowths in the experiment (F6) are around 320°C. Overall, aqueous or petroleum inclusions from quartz fracture usually have the highest T_h values of all the data. No correlation between the W/O ratio and the T_h of aqueous and petroleum inclusions have been found for both type of experiments.

A few T_m data were recorded for each experiment to verify the salinity of the trapped aqueous fluid. T_m values are between −3.8 and −3°C, which correspond to the NaCl molality of the starting aqueous solution, around 1 molal, using T_m-NaCl concentration and molality tables from Potter (1978).

4.3. Raman Microspectrometry

Methane in aqueous inclusions was only detected within a few of the fluid inclusion samples. Figure 5 shows Raman spectra of two synthetic aqueous inclusions, which were trapped inside quartz fractures from the GPA experiments (G1 and G2). Both have similar p-T trapping conditions with one inclusion (a) trapped in the H_2O-NaCl-CH_4 system, and the other aqueous inclusion (b) trapped in the H_2O-NH_4Cl-CH_4 system with petroleum. The presence of different ions explains the shift in the wave number of the maximum intensity of the water stretching band. The salting out effect is similar for all the monovalent cation chlorides. The cation effect has been described as negligible by Dubessy et al. (2002) who consider the anion as responsible for the breaking of the hydrogen bonds in water. By consequence, for equivalent molalities, NaCl and NH_4Cl should have the same effect on the methane solubility detection by Raman. The CH_4/H_2O ratio, and thus methane concentration, was lower when oil was present (mCH_4 = 0.13) than when oil was absent (mCH_4 = 0.3). Except for the G2 experiment, no methane was detected inside aqueous inclusions when oil was present.

4.4. Fourier Transform Infrared Microspectrometry (FT-IR)

FT-IR analysis was performed on individual petroleum inclusion and on the original oil sample, both before and after the experiments (Table 2). The alkanes values of the oil sample and the petroleum inclusions obtained by FT-IR are dependant on the CH_4 and CO_2 proportions. They cannot be compared to the saturated hydrocarbon (44% alkanes) values of the oil sample obtained by liquid chromatography before and after experiments, which are dependant on the aromatic and polar fractions. The only common parameter of both the oil sample and petroleum inclusions is the CH_2/CH_3 ratio.

In the GPA experiments, results show that FT-IR spectra of petroleum inclusions (250°C-212 bar) are very similar to those obtained for the oil sample before and after the corresponding experiments, with similar mean CH_2/CH_3 ratios of around 5.4. However, a methane contribution was detected in these petroleum inclusions, and has been quantified at 30 ± 5 mol%, independent of their location. Water and CO_2 were not found within the petroleum inclusions.

In the FPA experiments, calculated CH_2/CH_3 ratios are nonconstant and lower than those obtained in the GPA experiments. Mean CH_2/CH_3 ratios for the F1 to F5 experiments (350°C-400 bar) were calculated at around 3.1 ± 0.5 for petroleum inclusion and around 4.4 ± 0.2 for residual oil sample. This difference could be related to cracking processes during the experiments. Indeed, methane was detected within the gas and liquid phase inside synthetic petroleum inclusions, although methane was not added to these experiments (Fig. 6). FT-IR spectra of methane inside the gas phase of the inclusion shows P, Q, R branches that are characteristic of gas at very low pressure. The CO_2 content was calculated at around 0.4 ± 0.3 mol%, indicating that the oil has lost some C-O or C═O compounds. Although visible water was observed in

Table 2. FT-IR quantitative analysis of the petroleum inclusions and the oil sample before and after experiments. Mean CH_4, CO_2 and alkanes values are given in mol%. The CH_2/CH_3 ratio is the only common parameter for the free oil sample and the petroleum inclusions.

		Oil sample		Petroleum inclusions	
	Before exp.	G2 exp. (250°C-212 bar)	F1 to F5 exp. (350°C-400 bar)	G2 exp. 250°C-212 bar	F1 to F6 exp. 350°C-400 bar
CH_2/CH_3	5.4 ± 0.2	5.6 ± 0.2	4.4 ± 0.2	−5.8 ± 0.2	3.1 ± 0.5
$[CH_4]_m$	0	—	—	30 ± 5	20 ± 5
$[CO_2]_m$	0	—	—	0	0.4 ± 0.3
$[Alk]_m$	100	—	—	70 ± 5	80 ± 8

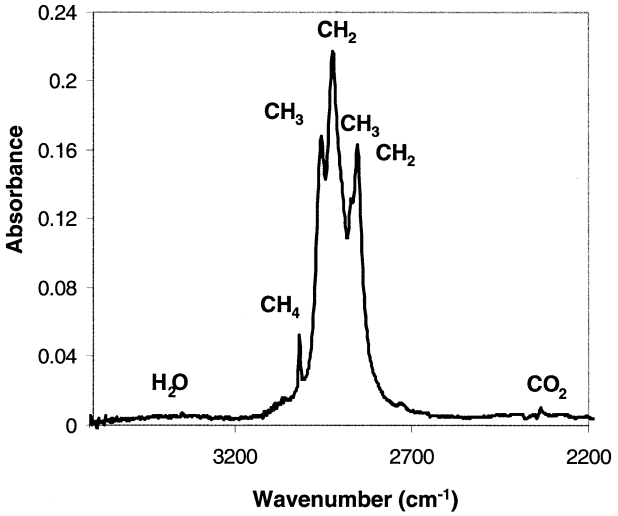

Fig. 6. FT-IR spectrum of a synthetic petroleum inclusion obtained in the gas phase at 25°C showing the presence of methane and traces of CO_2 (F3 experiment, W/O = 10/90; P, T_{max} = 350°C–400 bar, T_h = 295°C).

petroleum inclusions, vapour and/or liquid water was difficult to quantify by the FT-IR technique because of a superimposed water contribution from the thick quartz section, i.e., water from tiny aqueous inclusions below and/or above the analysed petroleum inclusion, and/or water adsorbed by the quartz crystal.

4.5. Confocal Scanning Laser Microscopy (CSLM)

Synthetic petroleum inclusions created with different W/O ratios (10/90, 20/80, 50/50) were analysed using CSLM. Maximum-recorded inclusion volume (oil and gas) was approximately 14000 μm^3 (F5 experiment, W/O = 50/50) and the minimum was 55 μm^3 (F3 experiments, W/O = 10/90). Vapour percentage at 20°C for liquid petroleum inclusions varies from 10.1 to 15.6% for GPA experiments, and between 13.4 to 29.5% for FPA experiments (Fig. 7). Volumetric calculations obtained from CSLM analysis demonstrate a positive

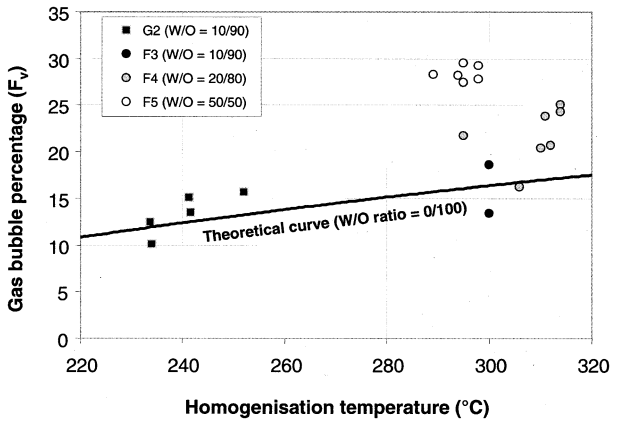

Fig. 7. F_v-T_h diagram of synthetic petroleum inclusions created in the GPA and FPA systems for different W/O ratios (10/90, 20/80 and 50/50). F_v values increase with increasing W/O ratios.

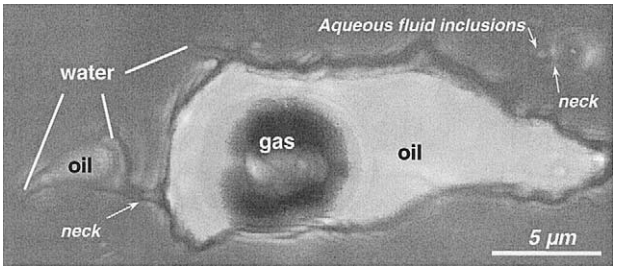

Fig. 8. CSLM microphotograph, obtained by mixing transmitted and UV light, showing two necked synthetic petroleum inclusions trapped inside a quartz microfracture (F4 experiment, 350°C-400 bar, W/O = 20/80).

evolution in the volume of the gas bubble (F_v) with the W/O ratio at 25°C imposed by the experimental conditions (Fig. 7). The higher the W/O ratio, the larger the volume of the gas bubble. CSLM observations, and photomicrographs obtained in reflection mode, reveal the presence of water inside petroleum inclusions that cannot be observed by conventional optical microscopy (Fig. 3c, Fig. 8). The water proportion inside a few of these petroleum inclusions was estimated between 27% (F4 experiments, W/O = 20/80) and 35% (F5 experiment, W/O = 50/50).

5. DISCUSSION

5.1. Effect of the W/O Ratio on Quartz Cementation and Fluid Inclusion Formation

Data from the literature show that water has a finite degree of solubility in hydrocarbon whatever the nature of the hydrocarbon (Pironon et al., 2000). The concentration of water in the hydrocarbon phase exponentially increases with temperature. Experimental data are variable at high temperature and reach ~1 wt.% of the hydrocarbon phase at 150°C, 1 to 4 wt.% at 200°C, 2 to 15 wt.% at 250°C, 4 to 50 wt.% at 300°C (Guerrant, 1964; Guillaume et al., 2001; Heidman et al., 1985; Kertes, 1989; Tsonopoulos and Wilson, 1983). Extrapolation of these experimental data at 350°C indicates that the amount of dissolved water into the oil phase varies between 10 to 100 wt.%. In the GPA system (<250°C), the dissolved amount of water into oil will thus evolve below 15 wt.% of water, mainly between 1 and 10 wt.%. In the FPA system (350°C), the amount of water into oil would be extremely variable, between 10 and 100 wt.%. For the lowest percentage (10%), two immiscible liquid phases are present in the FPA: oil (+ 10 wt.% of dissolved water) and water (+ *x* wt.% of dissolved oil). For the highest percentage (100%), only one liquid phase remains: oil (+ 100 wt.% of dissolved water). However, the oil-water system should be close to its critical point at 350°C, which should trend to an important miscibility (⩾10%). The variable W/O ratios observed in the fluid inclusions seems to indicate that these inclusions have been trapped in an immiscible oil-water domain.

Experiments carried out in the FPA (350°C-400 bar) have partially answered the question of the (eventual) inhibition of quartz cementation with high oil saturation. Quartz cementation process has been observed from a limited stage of growth with

Table 3. Mole percent composition of the oil sample and a synthetic fluid inclusion (G2 experiment) modelled by PIT software (Fig. 10). Cn_1: C_{11} to C_{15}, Cn_2: $C_{15}+$. The composition A and B is modelled using the T_h (242°C) and the F_v (13.4%) of the synthetic petroleum inclusions. The composition A and B has been obtained by chosen α and β values on the α-β curve generated by PIT, on the trend (A) and out of the trend (B) of the natural petroleum fluids (Fig. 9). The composition C is derived from the composition of the oil sample, adjusted with 34 mol% of CH_4 and normalised to fit with the experimental p-T conditions of the trapped petroleum inclusions (Fig. 10).

	Mol%			
Components	Oil sample	Comp A	Comp B	Comp C
C_1	0	10.4	26.18	34.05
C_2	0.03	1.57	3.53	0.02
C_3	0.17	2.57	3.87	0.11
iC_4	0.13	0.74	0.87	0.09
nC_4	0.55	1.66	1.95	0.37
iC_5	0.73	1.31	1.33	0.49
nC_5	1.25	2.11	2.14	0.83
C_6	4.90	4.06	2.79	3.23
C_7	7.08	4.38	3.00	4.67
C_8	7.48	4.32	2.87	4.93
C_9	7.27	4.27	2.75	4.80
C_{10}	6.81	4.21	2.65	4.48
Cn_1	27.93	31.10	20.38	18.42
Cn_2	35.66	27.30	25.70	23.52
α	—	0.951	0.962	—
β	—	0.219	0.523	—

the healing of quartz microfractures (W/O ratios from 0/100 to 50/50), to more advanced stages with the formation of quartz overgrowths (W/O ratios from 10/90 to 50/50). Larger overgrowths have reached up to 100 μm on core grains 1 cm in length). From these observations, a high oil saturation (>90 wt.%) does not inhibit quartz cementation at the p-T conditions of the experiments.

In the experiments, the formation of petroleum inclusions is dependant of the W/O ratio and is affected by the filling procedure of the gold tubes (i.e., water or oil first, inducing the presence of water or oil wetted quartz). When quartz was first wetted or partially wetted by water, quartz cementation and the fluid inclusion formation was enhanced. In contrast, petroleum inclusions were very rare (G3 and F1 experiments), or non-existent (G4 experiments), when quartz samples were first wetted by oil. Most of the petroleum and aqueous fluid inclusions were formed after maximum p-T conditions, during the decrease of temperature and pressure. Petroleum inclusions have been synthesised with W/O ratios ranging from 5/95 to 20/80 in the GPA experiments, and from 0/100 to 50/50 in the FPA experiments. In the FPA system, even if the W/O ratio is 0/100, we cannot assert that water is totally absent. First, we consider that the oil sample could plausibly contain a small amount of dissolved water. Second, synthetic quartz can contain irreducible water trapped inside its structure or inherited from the thermal fracturing of quartz during the water soaking process. Third, the silica gel could be another source of water because it should dehydrate at the temperatures of these experiments. The water contributed by the silica gel in the GPA experiments represents a small fraction of the total system, but it can be a large fraction of the water in the FPA capsules, especially if the initial W/O is low. The water proportion of the silica gel used in the capsules contains an average of 10 wt.% water. For the experiments with a initial W/O ratio of 5/95, 10/90, 20/80 and 50/50, the percentage of water contributed by the silica gel in the capsule could be up to a maximum of 40, 25, 15 and 10% respectively, which gives a "final W/O ratio" of 7/93, 13/87, 23/77 and 55/45 respectively.

5.2. PVTX Reconstruction Modelling

The aim of the PVTX reconstruction was to: (1) restore the trapping p-T conditions of the oil inside the inclusions; (2) generate a petroleum composition model consistent with the composition of the oil trapped inside the inclusion; and (3) validate the model with experimental data.

According to the experiments, oil trapped inside the petroleum inclusions could have different compositions. For the GPA experiments, the petroleum should correspond to a mixture of heavy alkanes (the oil sample) with dry gas (methane). For the FPA experiments, the methane that resulted from the cracking processes is taken into account. Methane contents generated by the model have been compared to those obtained in FT-IR, which is the only technique able to approximate the gas content of the petroleum inclusions. Both techniques share the same limitations; they do not completely take into account the aromatic and polar fractions. The CH_4 mol% determined by FT-IR is thus not strictly equivalent to the CH_4 mol% estimated by modelling (Tables 2 and 3), although both are very similar. On the other hand, PIT software does not take into account the presence of water inside petroleum inclusions. Therefore, PIT modelling results are only valid for the GPA petroleum inclusions because they contain less than 1–3% of water at the p-T trapping conditions (which do not affect PIT modelling), whereas those from the FPA experiments contained a lot of water, which can modify the slope of the isochore of the petroleum inclusions (Pironon et al., 2000).

The PIT (Petroleum Inclusion Thermodynamics) software (Thiéry et al., 2002) have been used to reconstruct the trapping conditions of synthetic petroleum fluid and oil composition. Two approaches have been adopted.

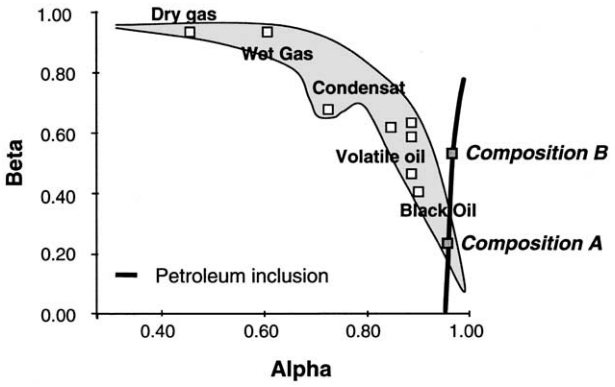

Fig. 9. α-β compositional diagram showing the trend of existing natural petroleum fluids from dry gas to black oil. The black α-β curve is modelled from PIT for a synthetic petroleum inclusion (T_h = 242°C; F_v = 13.4%). Two end-member values termed (A) and (B) have been chosen for this inclusion within the natural oil trend (A) and outside of this trend (B).

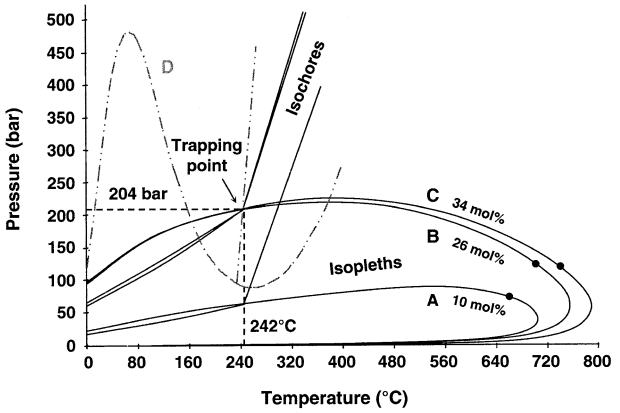

Fig. 10. P-T diagram of the modelled petroleum (T_h = 242°C; F_v = 13.4%) and contemporaneous aqueous (T_h = 237.3; CH_4 = 0.13 molal) fluid inclusions synthesised in the G2 experiment. Isopleths and isochores of the petroleum fluids (A, B and C with different mol% of CH_4) are calculated from PIT modelling, whereas those from the contemporaneous aqueous inclusion (D) are drawn using Duan et al. (1992) equations of state. The isopleths of the petroleum fluids have been modelled using an α-β couple chosen on the α-β curve generated by PIT (Fig. 9): (A) on the natural oil trend, (B) outside of the trend, and (C) by adjusting the composition of the starting oil sample with 34 mol% of methane. B and C fit with the trapping conditions of the synthetic petroleum inclusion at 242°C and 204 bar.

The first approach used T_h (242°C), acquired by microthermometry and the F_v (13.4%) acquired by CSLM from synthetic petroleum inclusions as input parameters. In this case, the p-T-X reconstruction modelled by PIT software is based on two parameters: α and β, which respectively represent the heavy fraction compounds ($\geq C_{10}$) and the methane plus the light alkanes (Thiéry et al., 2002). PIT modelling produces for each inclusion, a series of α, β solutions intersecting the natural oil and gas trend (Fig. 9). First, α and β were chosen at the intersect at point A (α_A = 0.951; β_A = 0.219). The isopleth A ("isocomposition") issued from the α_A, β_A modelling (Fig. 10) does not fit with the experimental conditions of trapping (242°C-204 bar). The cricondenbar of isopleth A is located at 87 bar and the related modelled composition is methane depleted at around 10 mol% CH_4 (model A, Table 3). These results show that model A does not reproduce the experimental conditions and the oil composition. Second, to simulate the experimental isopleth of the oil trapped at the experimental p-T conditions, another α, β solution (α_B = 0.962; β_B = 0.523) has been chosen (point B, Fig. 9). It is located away from the natural oil and gas trend. In this case, the composition modelling B gave a methane concentration of 26 mol% (Table 3), which is in accordance with the methane concentration determined from IR analyses (around 30 mol%). The composition B can be assimilated to a mixing of two fluids, one rich in methane and the other rich in heavy compounds. This mimics that of the experimental fluid composition.

The second approach was based on the known oil composition obtained by elementary analysis (oil sample, Table 3). In this case, no α-β parameters are required. The known oil sample composition (oil sample, Table 3) was progressively enriched with methane (model C, Table 3) until the p-T experimental conditions were reached (C, Fig. 10). The necessary methane concentration appears to be 34 mol% (model C, Table 3), which is near the methane concentration measured by FT-IR (around 30 mol%).

The oil composition issued from model B differs slightly from model C, which is based on the known oil sample composition (Table 3). This is explained by the presence of more C_2-C_5 fraction in the modelling B than in the modelling C. Although the composition of B and C are different, both isopleths (B, C) are similar up to 300°C. Results show that two different fluid compositions (model B and C) could have similar isopleths that match experimental trapping p-T conditions. The estimated methane concentrations range from 26 to 35 mol%.

5.3. Representativeness of Petroleum Fluid Inclusions

5.3.1. With the quartz cementation?

In many published cases of natural petroleum reservoirs, assemblages of fluid inclusions (i.e., trapped along the same growth zone or healed microfracture) show similar composition and T_h values. Even when the inclusions within a single overgrowth show variable T_h values, careful petrographic examination (SEM-CL) can reveal that fluid inclusions trapped in the same growth zone have similar T_h values (Burley et al., 1989; Rezaee and Tingate, 1997; Rossi et al., 2002). However, in more complex systems, fluid inclusions from the same CL zone, or a same quartz overgrowth, can sometimes display variable T_h, composition, gas filling and morphologies, even if they are spatially close to each other (Teinturier et al., 2002). According to the burial history of the reservoir, this difference could be explained by the combination of one, or several, processes: heterogeneous or homogeneous trapping of different fluids which migrated at different times, necking down or re-equilibration processes, and re-equilibration of quartz.

Fluid inclusions from one experiment have similar morphology, composition, and oil/vapour ratios. The range of T_h values can be variable according to the imposed *p*-T experimental conditions and the synthetic fluid inclusions could be representative of the quartz cementation along one p-T path. On the other hand, rare necking-down processes have been observed within microfractures and quartz overgrowths (parallel to the c axis of growth) in the FPA system (Fig. 8). When a 3-phase petroleum inclusion has been necked, the disconnected smaller inclusion, which usually contains water, appears to have migrated while its parent inclusion remains stationary. Indeed, many small monophase aqueous inclusions (<2 μm) occur in the latter stages of the quartz overgrowth, whereas petroleum inclusions are usually localised near the core-overgrowth boundary (Fig. 3a, b). The thermomigration of fluid inclusions has previously been observed in various KCl and NaCl crystals (Anthony and Cline, 1974; Muller, 1985) and in various crystals with oil (Kalyuzhnyy, 1982). Liquid-filled inclusions can migrate along an imposed thermal gradient by dissolution at the hot inclusion wall and reprecipitation at the cold wall. While the rate at which this process could happen would increase with higher temperatures and pressures (i.e., 350°C-400 bar), the rarity of the necked-down inclusions prevents any further conclusions to be drawn on the validity of such a migration process. The presence of these monophase aqueous inclusions in the quartz overgrowths could also be explained by metasta-

bility processes, which prevents physical nucleation of a gas bubble, particularly within small inclusions (Goldstein and Reynolds, 1994).

5.3.2. With the starting oil composition?

Comparison of the FT-IR spectra of the oil, both before and after the experiments with the associated petroleum inclusions, shows that, in an experimental system, fluid inclusion composition is very similar to the initial oil composition. From the CH_2/CH_3 ratio, which is the only measurable common parameter, the synthesized petroleum inclusions are representative of the parent oil up to 250°C and 212 bar (GPA experiments). PIT modelling of the oil inside synthetic petroleum inclusions, based on the known composition of the starting oil, the composition of methane, the T_h and the gas percentage (F_v), similarly suggests that the inclusions are representative of the parent oil. The number of inclusions, and hence the volume of oil, trapped in the quartz is not enough to use destructive techniques (GC-MS) for the acquisition, and comparison, of other parameters.

At higher temperatures, up to 350°C-400 bar (FPA experiments), oil sample and the oil inside the petroleum inclusions has evolved through cracking process (Teinturier et al., 2003). Indeed, the composition of oil has evolved to become relatively lighter, generating light alkanes and CH_4 whereas solid dark residues or bitumen has been found within the gold capsules (not observed in fluid inclusions) after FPA experiments. In natural diagenetic systems, cracking processes and the formation of such residual solids, should be extremely limited because oil rarely reaches temperatures higher than ~180°C.

5.3.3. With the experimental W/O ratio?

A theoretical curve of the gas bubble percentage (F_V) evolution with the homogenisation temperature (T_h) is shown in Figure 7, for the GPA (G2) and the FPA (F3, F4, F5) experimental conditions. This curve has been obtained using PIT software with the modelled composition of the oil in the petroleum inclusions from the GPA experiments. It does not take into account the presence of water and thus correspond to a W/O ratio of 0/100. Overall, most of the measured F_v values are higher than the theoretical F_v values. This could be related to the presence of dissolved water in the petroleum phase (§5.1.) and possibly to the methane enrichment with temperature or resulted from cracking (only in the FPA system).

For the GPA system, the measured F_v values of each petroleum inclusion lie between 10 and 16 vol.%, and are in general concordance with the predicted data. However, values of Fv at high T_h are higher than the modelled values. As seen before (§5.1.), the amount of dissolved water in the petroleum phase increases between 200 and 250°C, from 1 to 6 wt.%. Therefore, the higher the temperature, the more the Fv will move off the modelled tendency.

For the FPA system, a W/O ratio of 10/90 corresponds to a measured F_v of 13 to 18%; a W/O ratio of 20/80 corresponds to a F_v of 16 to 25%; a W/O ratio of 50/50 corresponds to a F_v of 27 to 30%. The variance of the measured Fv, with the theoretical Fv, becomes greater with an increase in the W/O ratio. This variance is about ±2.6% with a W/O of 10/90, from −0.8 to 8% with a W/O ratio of 20/80 and from 12.1 to 13.5% with a W/O ratio of 50/50. In the F3, F4 and F5 experiments, it appears that the W/O ratio plays the primary role in the evolution of the $F_{v,}$ compared to the effect of temperature. Indeed, petroleum inclusions from the F5 experiments have comparatively lower T_h and higher F_v values (Fig. 7). Water (vapour) can also be present in the gas phase at high p-T conditions but FT-IR analysis of the gas bubble is not sensitive enough to detect the presence of water vapour at low density, and therefore low pressure.

Is the W/O ratio imposed at the beginning of the experiment representative to the W/O ratio inside the trapped petroleum inclusions? The W/O ratio inside the petroleum inclusions cannot be easily determined as the CSLM technique does not permit the accurate determination of water volume in reflection mode. In addition, existing thermodynamic models do not take into account the presence of water for the reconstruction of the isopleth, the isochore and the oil composition, especially at the high p-T conditions of the experiments. Moreover, observed necking-down and possible thermal migration of fluid inclusions could significantly modify the W/O ratio.

5.4. The Methane: Where, When, Why and How?

In the FPA experiments CH_4 has been identified and quantified (approximately 20 mol%) by FT-IR analysis inside synthetic petroleum inclusions. As the original fluids were only oil and water, this CH_4 was most likely formed during the experiments through cracking process. Aqueous inclusions formed in the corresponding experiments do not contain methane.

In the GPA experiments, it appears as if the oil behaved as a barrier between the gas (upper) and water (lower) zones. Aqueous inclusions are methane undersaturated or absent when oil is present. The methane concentration is below its expected values for such GPA experimental conditions (Guillaume et al., 2003). In a p-T diagram, such behaviour is characterised by a shift of the aqueous isopleth (D, Fig. 10) to lower pressure as the oil isopleth becomes depleted with methane. The aqueous inclusion used for the modelling is located in a quartz microfracture spatially close (1 mm) to petroleum inclusions (G2 experiment). It is impossible to say if this aqueous inclusion is from the oil leg or the water leg due to the evolution of the oil-water contact during the G2 experiment, and to the migration of fluids under capillary pressure in the microfractures. The measured CH_4 molality (Raman) of the aqueous inclusion (T_h = 237.3°C) is 0.13 molal. In contrast, if the aqueous system was in equilibrium with the gas phase, the predicted CH_4 molality of this inclusion would be relatively high, around 0.3 molal and the aqueous isopleth would cross the p-T trapping point at around 242°C-204 bar. The absence or under-saturation of methane inside aqueous inclusions (GPA) could be related to the incomplete or the non-diffusion of methane into the aqueous phase. In other words, it seems possible that CH_4 diffusion inside the water was limited, reduced or stopped by the presence of oil. If the convection processes inside the GPA system is not efficient enough, the oil phase may be stratified from a heavy pole (at the water/oil interface) to a light pole (at the oil/gas interface). In this case, the water phase at the base of the autoclave should be equilibrated with the heaviest oil phase (methane-poor), and not with the gas phase. The infrared mea-

surements show that the methane concentration inside petroleum inclusions in GPA does not vary by much (± 5 mol%). This variation cannot be related to the location of the inclusions in the oil leg. We cannot prove disequilibrium during methane migration, but the oil stratification at the scale of the autoclave could be responsible for weak methane content variations. We suggest the following hypothesis: water in contact with oil is methane saturated in regard to the oil, and methane undersaturated in regard to the gas. The oil is methane saturated in regard to the gas phase. In a p-T diagram, the p-T trapping conditions of the experiment lie on the bubble point curve of the oil system and above the bubble curve of the aqueous system.

5.5. Relevance to Natural System

Experiments carried out in the gas pressure autoclave (GPA) and in the fluid pressure autoclave (FPA) show that the formation of fluid inclusions is dependant of the wettability of quartz to water or oil as well as the W/O ratio. The presence of oil did not prevent the formation of aqueous and petroleum inclusions from 185°C-163 bar up to 350°C and 400 bar for the duration of the experiment (<25 days). When the quartz was water-wet, high experimental p-T conditions have notably allowed the growth of quartz (which is not possible below 250°C) and the formation of fluid inclusions to occur, even with a high oil saturation (W/O ratios from 10/90 to 50/50). When quartz was oil-wet, quartz cementation was limited and inclusions were rare. It might be expected that similar conclusions could be formulated for p-T conditions in natural petroleum reservoirs and geological times. However, there are several problems that have to be considered. Although the lowest GPA experimental p-T conditions can be extrapolated to natural systems, high FPA experimental temperature conditions (required to form quartz overgrowth in laboratory) are difficult to extrapolate to low diagenetic temperatures. First, the solubility of water in oil is many times greater at the experimental temperatures than at diagenetic temperatures, implying that processes requiring water will be enhanced excessively at these high temperatures. Second, the mechanism of reaction should be different at these high experimental temperatures. In diagenetic reservoirs, rocks respond to the effective stress (difference between the lithostatic and the fluid pressure), and the main mechanism responsible for the silica supply is caused by pressure-dissolution processes (quartz-quartz contact). In our experimental closed system (gold capsules), the effective stress is equivalent to the fluid pressure where no oriented strain is applied. The high fluid pressures would thus not make the system completely representative of the subsurface. The silica in the experiments comes from the silica gel and from the quartz itself (Teinturier and Pironon, in press). High fluid pressures arguably serve to counteract quartz cementation through the negative effect on pressure solution. However, high pressures also increase the solubility of quartz, and the decrease of temperatures at constant pressure during the experiments allows the quartz to precipitate faster by accelerating the attainment of fluid equilibrium and oversaturation process.

On the other hand, if an oil leg acts as a barrier between a gas and a water leg (like in the experiment), some of the aqueous inclusions associated with petroleum inclusions could be methane-undersaturated. The eventual effect of petroleum on methane diffusion into water phase could thus explain the variable methane content of aqueous inclusions in natural petroleum reservoirs. The segregation and local variation of the oil/gas/water column could increase the possible inhibition of petroleum on gas diffusion into the water phase. Bearing in mind that the oil sample used in the experiments is relatively heavy and depleted in C_2-C_5; this effect could be minimised with lighter oil such as gas condensate or volatile oil. If aqueous inclusions are methane undersaturated when heavy oil is present, then the hypothesis used by thermodynamic models, that the aqueous fluid is always methane saturated, is incorrect. In this case, the use of the isotherm from the T_h of the aqueous inclusions should be avoided in reconstructions of the p-T trapping conditions of heavy oils. If possible, isopleths and isochores of the aqueous system should be modelled using the CH_4 molality (Raman), the salinity and the T_h (microthermometry) of contemporaneous aqueous inclusions.

6. CONCLUSIONS

The presence of fluid inclusions is a good indicator of the conditions of quartz growth. This work demonstrates that GPA and FPA systems can simulate the growth of quartz and the trapping of fluid inclusions, even if the temperature required to counterbalance the slow kinetic-growth of the crystals is high (≥200°C). Both fluid inclusions and quartz overgrowth have formed, even at oil saturations of greater than 90%. Petroleum inclusions have been synthesised in quartz microfractures (W/O ratios from 0/100 to 50/50; 209–350°C; 175–400 bar) and also in quartz overgrowths (W/O ratios from 10/90 to 50/50; 289–350°C; 350–400 bar). Aqueous inclusions have been synthesised in the presence of oil inside quartz microfractures from 185°C-163 bar up to 350°C-400 bar, and inside quartz overgrowths from 277°C-330 bar. Synthesised petroleum inclusions seem representative of the parent oil up to 250°C in our experiments. Aqueous inclusions are methane undersaturated when oil is present, which acts as a barrier between the gas and the water phase and limiting methane diffusion. Therefore, reconstructions of the p-T trapping conditions of heavy oil using isotherms from the T_h of aqueous inclusions should be avoided. At 350°C, evidence for cracking process has been observed with the consequent generation of methane. In addition, observed necking-down and possible thermal migration of fluid inclusions at high temperature might have modified the W/O ratio of the inclusions.

This preliminary study may be the first step for new and further developments on the studies of the trapping of petroleum and aqueous inclusions in quartz. The presence of water in the petroleum phase has an effect on the PVTX properties and the modelling of the isopleth/isochore of petroleum inclusions, especially above 250°C where the solubility of water into the petroleum phase increases. Such an approach could also be used to simulate and characterise the cracking process of organic matter. The data from this fluid inclusion study will be compared to the crystal chemistry investigated in Part II (Teinturier and Pironon, in press), to determine the precise conditions of quartz growth in presence of natural hydrocarbons.

Acknowledgments—We would like to express our thanks to reviewers Carlos Rossi, Hsin-Yi Tseng, Richard Worden and associate editor Robert Burruss for their constructive reviews and valuable comments.

Richard Kempton from CSIRO Petroleum is thanked for providing thoughtful suggestions and improving the manuscript. We also thank Frédéric Walgenwitz from Total for his helpful support and Jérôme Mutterer from the IBMP laboratory for his active participation to CSLM analyses.

Associate editor: R. C. Burruss

REFERENCES

Aplin A. C., MacLeod G., Larter S. R., Pedersen K. S., Sorensen H., and Booth T. (1999) Combined use of Confocal Laser Scanning Microscopy and PVT simulation for estimating the composition and physical properties of petroleum in fluid inclusions. *Mar. Petrol. Geol.* **16,** 97–110.

Anthony T. R. and Cline H. E. (1974) Thermomigration of liquid droplets in salt, 4th Symposium on Salt. *North. Geol. Soc.* **1,** 313–321.

Barclay S. A., Worden R. H. (2000) Effects of reservoir wettability on quartz cementation in oil fields. In *Quartz cementation in sandstones. Special publication of the International Association of Sedimentologists* (ed. R. H. Worden, S. Morad), *Blackwell Science*, 29, 103–117.

Bodnar R. J. and Sterner S. M. (1985) Synthetic fluid inclusions in natural quartz. III. Determination of phase equilibrium properties in the system H_20-NaCl to 1000°C and 1500. *Geochim. Cosmochim. Acta* **49,** 1861–1873.

Brown P. E. (1989) FLINCOR: A microcomputer program for the reduction andinvestigation of fluid inclusion data. *Am. Mineral.* **74,** 1390–1393.

Burley et al. (1989) Timing diagenesis in the Tartan Reservoir (UK North Sea): constraints from combined cathodoluminescence microscopy and fluid inclusion studies. *Mar. Petrol. Geol.* 6, 98–104.

Chabiron A., Pironon J., Massare D. (2004) Characterisation of water in synthetic rhyolitic glasses and natural melt inclusions by Raman spectroscopy. *Contrib. Mineral. Petrol.* **146,** 485–492.

Dixon S. A., Summers D. M., and Surdam R. C. (1989) Diagenesis and prservation of porosity in Norphlet Formation (Upper Jurassic), southern Alabama. *Am. Assoc. Petrol. Geol. Bull.* **73,** 707–728.

Duan Z., Moller N., J. H. W. (1992) An equation of state (EOS) for CH_4, CO_2 and H_2O. *Geochim. Cosmoschim. Acta* **56,** 2605–2618.

Dubessy J., Buschaert S., Lamb W., Pironon J., and Thiery R. (2000a) Methane-bearing aqueous fluid inclusions: Raman analysis, thermodynamic modelling and application to petroleum basins. *Chem. Geol.* **173 (***1***),** 193–205 3.

Dubessy J., Guillaume D., Buschaert S., Fabre C., and Pironon J. (2000b) Production of synthetic fluid inclusions in the H_2O-CH_4-NaCl system using laser-ablation in fluorite and quartz. *Eur. J. Mineral.* **12 (***6***),** 1083–1091.

Dubessy J., Lhomme T., Boiron M. C., and Rull F. (2002) Determination of chlorinity in aqueous fluids using Raman spectroscopy of the stretching band of water at room temperature: Application to fluid inclusions. *Appl. Spectros.* **56,** 99–106.

Dubois M., Weisbrod A., and Shtuka A. (1994) Experimental determination of the two-phase (liquid and vapour) region in water-alkali chloride binary systems at 500 et 600°C using synthetic fluid inclusions. *Chem. Geol.* **115,** 227–238.

Gluyas J. G., Robinson A. G., Emery D., Grant S. M. and Oxtoby N. H. (1993) The link between petroleum emplacement and sandstone cementation. In *Petroleum Geology of Northwest Europe: Proceedings of the 4th Conference.* (ed. J. R. Parker) pp. 1395–1402. Geol. Soc. Lond.

Goldstein R. H. and Reynolds T. J. (1994) Systematics of fluid inclusions in diagenetic minerals. *SEPM Short Course.* **31,** 199 p..

Guerrant R. P (1964) Hydrocarbon-water solubilities at high temperatures under vapor-liquid-liquid equilibrium conditions, PhD Thesis, Pennsylvania State University, 124p.

Guillaume D., Tkachenko S., Dubessy J., and Pironon J. (2001) High-temperature and high-pressure water solubility in ethylbenzene to 200°C and 1 kbar and the acetic acid effect. *Geochim. Cosmochim. Acta* **65 (***19***),** 3319–3324.

Guillaume D., Teinturier S., Dubessy J., and Pironon J. (2003) Calibration of methane analysis by Raman spectroscopy in H_2O-NaCl-CH_4 fluid inclusions. *Chem. Geol.* **194,** 41–49.

Haszeldine R. S. and Osborne M. (1993) Fluid inclusion temperatures in diagenetic quartz reset by burial: implications for oil field cementation. *Am. Assoc. Petrol. Geol. Bull.* **36,** 35–46.

Heidman J. L., Tsonopoulos C., Brady C., and Wilson G. M. (1985) High-temperature mutual solubilities of hydrocarbons and water. Part II: ethylbenzene, ethylcyclohexane, and n-octane. *Am. Instit. Chem. Eng. J.* **31,** 376–384.

Kalyuzhnyy V. A. (1982) Fundamental studies of mineral-forming fluids. Izd. Nauk. Dumka, Kiev, USSR. 225 p.

Kertes A. S. (1989) IUPAC Solubility data series. Hydrocarbons with water and seawater. Part II: C_8 to C_{36}. Pergamon Press, New York, (ed. David G. Shaw) vol. 38.

Lamb W. M., Popp R. K., and Boockoff L. A. (1996) The determination of phase relations in the CH_4-H_2O-NaCl system at 1 kbar, 400 to 600°C using synthetic fluid inclusions. *Geochim. Cosmochim. Acta* **60,** 1885–1897.

Larese R. E. and Hall D. L. (1996) Studying petroleum migration with fluid inclusions: results from hydrothermal burial simulation experiments. *PACROFI VI.* 74–75.

Marchand A. M. E., Haszeldine R. S., Smalley P. C., Macaulay C. I., and Fallick A. E. (2001) Evidence for reduced quartz-cementation rates in oil-filled sandstones. *Geology* **29,** 915–918.

Marchand A. M. E., Smalley P. C., Haszeldine R. S., and Fallick A. E. (2002) Note on the importance of hydrocarbon fill for reservoir quality prediction in sandstones. *Am. Assoc. Petrol. Geol. Bull.* **86,** 1561–1571.

Meunier J. D. (1992) Precipitation of minerals between detrital quartz and quartz overgrowths in sandstones. *Eur. J. Mineral.* **4,** 1401–1406.

Midtbø R. E. A., Rykkje J. M., and Ramm M. (2000) Deep burial diagenesis and reservoir quality along the eastern flank of the Viking Graben. Evidence for illitization and quartz cementation after hydrocarbon emplacement. *Clay Miner.* **35,** 227–237.

Muller E. (1985) The transportation of brine inclusions in rock salt in a temperature field of a heat source. *Cryst. Res. Technol.* **20 (***5***),** 677–682.

Pironon J. (1990) Synthesis of hydrocarbon fluid inclusions at low temperature. *Am. Mineral.* **75,** 226–229.

Pironon J., Canals M., Dubessy J., Walgenwitz F., and Laplace-Builhe C. (1998) Volumetric reconstruction of individual oil inclusions by confocal scanning laser microscopy. *Eur. J. Mineral.* **10,** 1143–1150.

Pironon J., Thiéry R., Teinturier S., and Walgenwitz F. (2000) Water in petroleum inclusions: evidence from Raman and FT-IR measurements, PVT consequences. *J. Geochem. Explor.* **69,** 663–668 70.

Pironon J., Thiery R., Ayt Ougougdal M., Teinturier S., Beaudoin S., and Walgenwitz F. (2001) FT-IR measurements of petroleum fluid inclusions: methane, n-alkanes and carbon dioxide quantitative analysis. *Geofluids* **1,** 2–10.

Poty B., Leroy J., and Jachimowicz L. (1976) Un nouvel appareil pour la mesure des températures sous le microscope: l'installation de microthermométrie Chaixmeca. *Bull. Soc. Fr. Minéral. Cristallogr.* **99,** 182–186.

Potter R. W., II, Clynne M. A., and Brown D. L. (1978) Freezing point depression of aqueous sodium chloride solutions. *Econ. Geol.* **73,** 284–285.

Ramm M. (1992) Porosity-depth trends in reservoir sandstones: theoretical models related to Jurassic sandstones, offshore Norway. *Mar. Petrol. Geol.* **9,** 324–327.

Rezaee M. and Tingate P. R. (1997) The origin of quartz cement in the Tirrawarra Sandstone, southern Cooper Basin, South Australia. *J. Sediment. Res., Section A: Sedimentary Petrology and Processes* **67,** 168–177.

Roedder E. and Kopp O. C. (1975) A check on the validity of the pressure correction in inclusion geothermometry, using hydrothermally grown quartz. *Fortschr. Mineral.* **52,** 431–446.

Rossi C., Goldstein R. H., Ceriani A., and Marfil R. (2002) Fluid inclusions record thermal and fluid evolution in reservoir sandstones, Khatatba Formation, Western Desert, Egypt: A case for fluid injection. *Am. Assoc. Petrol. Geol. Bull.* **86,** 1773–1799.

Saigal G., Bjorlykke K., and Larter S. (1992) The effects of oil emplacement on diagenetic processes—Examples from the Fulmar reservoir sandstones, Central North Sea. *Am. Assoc. Petrol. Geol. Bull.* **76,** 1024–1033.

Sawaki T., Sasada M., Sasaki M., Tsukimura K., Hyodo M., Okabe T., Uchida T., and Yagi M. (1997) Synthetic fluid inclusion logging to measure temperatures and sample fluids in the Kakkonda geothermal field, Japan. *Geothermics* **26,** 281–303.

Shelton K. L. and Orville M. O. (1980) Formation of synthetic fluid inclusions in natural quartz. *Am. Mineral.* **65,** 1233–1236.

Stasiuk L. D. and Snowdon L. R. (1997) Fluorescence micro-spectrometry of synthetic and natural hydrocarbon fluid inclusions: crude oil chemistry, density and application to petroleum migration. *Appl. Geochem.* **12,** 229–241.

Sterner S. M. and Bodnar R. J. (1984) Synthetic fluid inclusions in natural quartz I. Compositional types synthesized and applications to experimental geochemistry. *Geochim. Cosmochim. Acta* **48,** 2659–2668.

Teinturier S., Pironon J., and Walgenwitz F. (2002) Fluid inclusions and PVTX modelling: Examples from the Garn Formation in well 6507 2/2, Haltenbanken, Mid-Norway. *Mar. Petrol. Geol.* **15,** 755–765.

Teinturier S., Elie M., and Pironon J. (2003) Evidence of oil cracking using synthetic petroleum inclusion. *J. Geochem. Explor.* **78,** 421–425 79.

Teinturier S. and Pironon J. (2003) Synthetic fluid inclusions as recorders of microfracture healing and overgrowth formation rates. *Am. Mineral.* **88,** 1204–1208.

Tester J. W., Worley W. G., Robinson B. A., Grigsby C. O., and Feerer J. (1994) Correlating quartz dissolution kinetics in pure water from 25 to 625°C. *Geochim. Cosmochim. Acta* **58,** 2407–2420.

Thiéry R., Pironon J., Walgenwitz F., and Montel F. (2002) Individual characterization of petroleum fluid inclusions (composition and P-T trapping conditions) by microthermometry and confocal laser scanning microscopy: inferences from applied thermodynamics of oils. *Mar. Petrol. Geol.* **19,** 847–859.

Tsonopoulos C. and Wilson G. M. (1983) High-temperature mutual-solubilities of hydrocarbons and water. Part I: benzene, cyclohexane and n-hexane. *Am. Inst. Chem. Eng. J.* **61,** 815–817.

Vityk M. O., Pottorf R. J., Gray G. G., Larese D. and Hall D. (2001) Application of synthetic fluid inclusions to hydrocarbon system analysis. *ECROFI XVI.* 455–456.

Walderhaug O. (1990) A fluid inclusion study of quartz-cemented sandstones from offshore mid-Norway—possible evidence for continued quartz cementation during oil emplacement. *J. Sed. Petrol.* **60,** 203–210.

Worden R. H., Morad S. (2000) Quartz cementation in oil field sandstones: a review of the key controversies. In *Quartz cementation in sandstones. Special Publication of the International Association of Sedimentologists* (ed. R. H. Worden, S. Morad). Blackwell Science, 29, 1–20.

Xie Z. and Walther J. V. (1993) Quartz solubilities in NaCl solutions with and without wollastonite at elevated temperatures and pressures. *Geochim. Cosmochim. Acta* **57,** 1947–1955.

Zhang Y. G. and Frantz J. D. (1987) Determination of the homogenisation temperatures and densities of supercritical fluids in the system NaCl-KCl-$CaCl_2$-H_2O using synthetic fluid inclusions. *Chem. Geol.* **64,** 335–350.

Teinturier S. and Pironon J. (in press). Experimental growth of quartz in petroleum environment. Part 2: Solid-liquid interaction. *Geochim. et Cosmochim. Acta*.